Treatment with human placental extracts inhibits allergic rhinitis by modulating AMPK/SHP1/SHP2/STING signaling

BEIBEI WO[1], SHUANG LIU[2], ZIHUI LIANG[3] and XIAOMING LI[1]

[1]Department of Otolaryngology Head and Neck Surgery, Hebei Medical University, Shijiazhuang, Hebei 050011, P.R. China; [2]Department of Pathology, The 980th Hospital of People's Liberation Army (PLA) Joint Logistics Support Force, Shijiazhuang, Hebei 050082, P.R. China; [3]Department of Surgery, Hebei Medical University, Shijiazhuang, Hebei 050011, P.R. China

Received September 3, 2024; Accepted March 11, 2025

DOI: 10.3892/mmr.2025.13548

Abstract. The present study aimed to investigate the regulatory effects and mechanisms of human placental extracts (HPE) on rats and cell models of ovalbumin (OVA)-induced allergic rhinitis (AR). IFN-y and LPS induced AR *in vitro*. A total of 32 male Sprague-Dawley (SD) rats were randomly divided into the following four groups: Sham group, model group, model + HPE group and model + HPE + AMPK inhibitor group (n=8 rats/group). With the exception of the sham group, the remaining three groups were sensitized with OVA to establish an AR model, followed by various treatments. Hematoxylin and eosin staining was utilized to observe morphological changes in the nasal mucosa, ELISA was employed to measure serum levels of IL-1β, interferon (IFN)β, immunoglobulin (Ig)E, IgG1 and IgG2a, and western blotting was conducted to assess protein expression across the groups. The sham group exhibited intact tissue structure with no notable pathological alterations. The model group demonstrated pronounced pathological features, including extensive infiltration of inflammatory cells, tissue shedding and edema. The model + HPE group revealed a gradual restoration of tissue architecture, characterized by reduced edema and inflammatory infiltration, whereas the model + HPE + AMPK inhibitor group again exhibited significant inflammatory cell infiltration and other pathological manifestations. Compared with the sham operation group, the levels of IL-1β, IFNβ, IgE, IgG1 and IgG2a in the serum of the model group were elevated. The levels of IL-1β, IFNβ, IgE, IgG1 and IgG2a in the model + HPE group were lower than those in the model group. In addition, the levels of IL-1β, IFNβ, IgE, IgG1 and IgG2a in the model + HPE + AMPK inhibitor group were higher than those in the model + HPE group. Relative to the sham group, the expression levels of phosphorylated (p)-AMPK/total (t)-AMPK, p-Src homology 2-containing phosphatase (SHP)1/t-SHP1 and p-SHP2/t-SHP2 were diminished, whereas the expression levels of p-STING/t-STING and p-TBK1/t-TBK1 were heightened in the model group. In comparison to the model group, the expression levels of p-AMPK/t-AMPK, p-SHP1/t-SHP1 and p-SHP2/t-SHP2 were enhanced, whereas the expression levels of p-STING/t-STING and p-TBK1/t-TBK1 were reduced in the model + HPE group. Conversely, when compared with the model + HPE group, the expression levels of p-AMPK/t-AMPK, p-SHP1/t-SHP1 and p-SHP2/t-SHP2 were decreased, whereas those of p-STING/t-STING and p-TBK1/t-TBK1 were increased in the model + HPE + AMPK inhibitor group. In conclusion, HPE may inhibit AR by modulating the AMPK/SHP1/SHP2/STING signaling pathway.

Introduction

Allergic rhinitis (AR) is a chronic inflammatory disease of the nasal cavity mediated by immunoglobulin (Ig)E, characterized by typical symptoms such as sneezing, nasal itching, nasal congestion and rhinorrhea, which severely affect patient quality of life (1,2). The key mechanism underlying the pathogenesis of AR is a hypersensitivity reaction triggered by specific allergens coming into contact with the nasal mucosa. Allergen exposure induces the recruitment of various immune cells, including eosinophils, mast cells, basophils and neutrophils, into the nasal mucosa, activating epithelial cells, fibroblasts and T helper 2 (Th2) cell responses. This leads to the release of numerous pro-inflammatory mediators, such as IL-4, IL-5 and IL-13, which trigger B cells to produce antigen-specific IgE, further activating mast cells and basophils, resulting in nasal mucosal allergy and inflammation (3,4).

Human placental extracts (HPE) refer to a range of small bioactive molecules extracted from the human placenta (5). Previous studies have shown that HPE is rich in active substances, such as nutritional factors, cytokines, DNA materials, neuropeptides, enkephalins, polysaccharides, amino acids, proteins, lipids and trace elements (6-8). These substances have pharmacological effects, including enhancing the body's energy metabolism (9), promoting neurovascular growth, combating fatty liver, exerting antioxidant effects, modulating the immune system and exerting anti-inflammatory actions (10).

Correspondence to: Professor Xiaoming Li, Department of Otolaryngology Head and Neck Surgery, Hebei Medical University, 361 Zhongshan East Road, Shijiazhuang, Hebei 050011, P.R. China
E-mail: 18100093@hebmu.edu.cn

Key words: human placental extracts, AMPK/SHP1/SHP2/STING, ovalbumin, allergic rhinitis

AMPK is an energy-sensing enzyme that plays a vital role in regulating cellular metabolism and energy balance. Activating AMPK can directly phosphorylate the p65 subunit of NF-κB. The phosphorylated p65 subunit has a reduced ability to bind to DNA, thereby inhibiting the transcriptional activity of NF-κB and reducing the expression of downstream inflammation-related genes such as tumor necrosis factor-α (TNF-α) and interleukin-6 (IL-6), thereby reducing the inflammatory response. Since AR is an allergic inflammatory disease, activating AMPK may reduce inflammation of the nasal mucosa and alleviate symptoms. AMPK activation may also improve the local immune environment, thereby reducing the severity of allergic reactions (11).

NF-κB refers to a family of transcription factors widely present in mammalian cells, which have a key role in regulating immune responses, inflammatory reactions, cell survival, proliferation and differentiation. NF-κB can act on Src homology 2-containing phosphatase (SHP)1 and SHP2 signaling molecules through various stimuli (12-14). SHP1 is a powerful anti-inflammatory factor, and it has been reported that the astrocytes from SHP1 gene-deficient mice exhibit a stronger inflammatory response under stimulation by interferon (IFN) and lipopolysaccharide (LPS) (15). SHP2 is a non-receptor protein tyrosine phosphatase expressed in various cell types that regulates multiple signaling pathways. The regulatory role of SHP2 may balance inflammatory responses by inhibiting or promoting the NF-κB pathway. For example, it has been reported that SHP2 indirectly affects the activation level of NF-κB by regulating the activity of RTK to regulate the intensity and duration of the inflammatory response (16). The present study aimed to evaluate the relationship between AMPK and NF-κB, as well as the role of SHP1 and SHP2 in AR.

Materials and methods

Experimental animals. A total of 32 male Sprague-Dawley (SD) rats (age, 4-5 weeks; weight, 200-220 g) were purchased from Henan SKBS Biotechnology Co., Ltd (http://www.hnskbs.com/). [animal production license no. SCXK (Yu) 2020-0005]. All experiments were approved by the Animal Protection and Use Committee of Hebei Medical University [Shijiazhuang, China; approval no. Institutional Animal Care and Use Committee (IACUC)-Hebmu-P-2024024], and were conducted in accordance with the laboratory animal husbandry regulations and ethical requirements of Hebei Medical University. All methods were performed in accordance with the relevant guidelines and regulations. and conformed to the principle of the 3Rs and ARRIVE guidelines (17). The rats were housed in specific pathogen-free-grade animal facilities with a temperature of 23±1˚C and relative humidity of 55±2%, with free access to food and water. The rats were raised in a 12-h light/dark cycle.

Experimental materials. Fetal bovine serum (FBS) and DMEM were obtained from Gibco; Thermo Fisher Scientific, Inc. Ovalbumin (OVA) was purchased from MilliporeSigma. HPE was obtained from Handan Kangye Pharmaceutical Co., Ltd. The ELISA kit includes Interleukin-1β (IL-1β) (PI303, Beyotime), Interferon-β (IFNβ) (E-EL-R0545, Elabscience), Interferon-α (IFNα) (E-EL-R3036, Elabscience), malondialdehyde (MDA) (S0131S, Beyotime), superoxide dismutase (SOD) (E-EL-R1424, Elabscience), Immunoglobulin E (IgE) (E-EL-R0517, Elabscience), Immunoglobulin G1 (IgG1) (88-50500-88, Thermo Fisher Scientific), Immunoglobulin G2a (IgG2a) (E-EL-R2415, Elabscience) and glutathione (GSH) (E-EL-0026, Elabscience). The AMPK inhibitor dorsomorphin 2HCl and Transwell chambers were obtained from Beijing Baiolaibo Technology Co., Ltd. The SHP2/SHP1 inhibitor NSC-87877 and the STING agonist DMXAA were purchased from MedChemExpress. Western blot electrophoresis equipment was purchased from Shanghai Sevier Technology Co., Ltd (https://www.servier.com.cn/).

Kyoto encyclopedia of genes and genomes (KEGG) pathway analysis of key biological pathways. The AR dataset GSE44037 (18) was downloaded from the Gene Expression Omnibus (GEO) database (URL: http://example.com/gse44037); this dataset includes five AR samples and six healthy control samples. For data preprocessing, R software (version 4.0.3.; https://www.r-project.org) was used to normalize RNA sequencing data using log2 transformation Microarray data from the GEO dataset were background corrected, normalized and averaged using robust multi-array analysis. The processed data were then batch-effect corrected using the ComBat (https://bioconductor.org/packages/release/bioc/html/sva.html) method. The AR dataset GSE44037 included five samples of patients with AR-related disorders and six samples of healthy controls. The limma package (https://bioconductor.org/packages/release/bioc/html/limma.html) was utilized for identifying differentially expressed genes (DEGs) between the AR samples and healthy controls; DEGs between these groups were identified with |log2 fold change|>1 and $P<0.05$. P-values were adjusted for multiple hypotheses using the Benjamini-Hochberg method. Gene Ontology (GO) and KEGG pathway enrichment analyses were performed using the ClusterProfiler package (version 3.18.1; https://bioconductor.org/packages/release/bioc/html/clusterProfiler.html). GO analysis identified enriched cellular component (CC), molecular function (MF) and biological process (BP) terms, whereas KEGG pathway analysis identified key biological pathways. Spearman correlation analysis was performed to assess the correlation among DEGs. This analysis helps to identify relationships between the expression levels of DEGs in the context of AR-related disorders and healthy controls.

Construction of a rat model of AR. A total of 32 male rats were randomly divided into the following four groups (n=8 rats/group): Sham, model, model + HPE and model + HPE + AMPK inhibitor groups. Modeling of AR in rats was performed according to a previous study (19). The AR rat model was established as follows: i) Sensitization phase: OVA solution [0.3 mg OVA and 30 mg $Al(OH)_3$ in 1 ml 0.9% saline] was administered intraperitoneally on days 1, 3, 5, 7, 9, 11 and 13, totaling seven injections. ii) Challenge phase: On days 15-17, a 50 mg/ml OVA solution (50 mg OVA in 1 ml 0.9% saline) was administered intranasally, 20 μl/rat; and on days 18-21, a 100 mg/ml OVA solution (100 mg OVA in 1 ml 0.9% saline) was administered intranasally, 20 μl/rat. The sham group received the same volume of saline or $Al(OH)_3$ solution.

Once the AR model was established, interventions with HPE or an AMPK inhibitor were administered. The model + HPE group received intraperitoneal injections of 5 ml/kg HPE solution, from days 28-46. The model + HPE + AMPK inhibitor group received intravenous injections of 10 mg/kg AMPK inhibitor solution and 5 ml/kg HPE solution intraperitoneally, from days 28 to 46. Follow-up experiments were conducted after 46 days. At least once a day, the health of the rats was thoroughly inspected, including skin, fur, eyes, nose, mouth, ears, limbs, tail and abdomen. The rats were weighed weekly to monitor growth and development or disease progression. Food and water consumption was checked daily, and rats were observed for behavior, including activity levels, social interactions, eating and drinking habits, and exploratory behavior.

After subsequent H&E experiments and ELISA tests, the rats were euthanized using CO_2 (30% vol/min CO_2). The rats were exposed to CO_2 until they lost consciousness and were maintained in that environment for 20 min to confirm death. The exposure time was 1-3 min. CO_2 was delivered into a well-sealed chamber of an appropriate size for the rats to ensure the CO_2 concentration met the specified standard. The behavior of the rats was monitored to ensure they quickly lost consciousness. During the euthanasia process, a quiet, softly lit room was used, avoiding a noisy environment and strong light stimulation, and warm mats or towels were used to wrap the rats to ensure they were comfortable; rough movements were avoided during the operation. The staff performing euthanasia were professionally trained and familiar with the operation procedure, and were able to complete the operation quickly and effectively, reducing the pain and fear of the animals. Successful euthanasia was confirmed 20 min after the heartbeat of the rats could no longer be detected. Euthanasia was preceded by gas anesthesia with 4.5% isoflurane to reduce anxiety in the rats. This euthanasia procedure followed the guidelines of the IACUC or Animal Protection and Use Committee of Hebei Medical University. In addition, if the rats showed loss of appetite and depression, the experiment was terminated and the rats were sacrificed. The procedures used in the present study minimized animal suffering, and the bodies of the rats were properly disposed of after the process.

Hematoxylin and eosin (H&E) staining of morphological changes in nasal mucosa. The rats were first induced under gas anesthesia with 4.5% isoflurane and then anesthesia was maintained with 2% isoflurane. After anesthetizing the rats, the nasal mucosa tissues were isolated, fixed with 4% paraformaldehyde for 24 h at room temperature, dehydrated with ethanol and embedded in paraffin. Paraffin-embedded sections (5 μm) were deparaffinized twice at room temperature using xylene for 5 min each time, in 100, 90, 80 and 70% ethanol for 5 min each, and in distilled water for 5 min. The distilled water was removed, and the sample was stained with hematoxylin for 15 min at room temperature. Subsequently, the hematoxylin was removed with running water and differentiation was carried out at room temperature with 1% hydrochloric acid in alcohol for 3 sec, followed by washing with water. The sample was then immersed in running water to remove the blue color for 10 min. One drop of 0.5% eosin was added, and the sample was stained for 1 min at room temperature. Subsequently, dehydration was carried out with 80, 90, 95 and 100% ethanol, two xylene washes (5 min each) were carried out and the tissue was left to dry at room temperature. A drop of neutral gum was then added to the tissue and the cover glass was sealed at room temperature. After 24 h, the tissue was observed under an optical microscope and images were captured.

ELISA. Rats were anesthetized with 4.5% isoflurane gas to induce anesthesia and then maintained with 2% isoflurane to collect 1.5 ml of blood from the abdominal aorta, after which, serum was separated by centrifugation. The serum was centrifuged at 1,200 x g for 10 min. separated to obtain serum. placed at 4˚C for 30 min. The rats were then euthanized using CO_2 at a flow rate of 30% container volume/min, and euthanasia was verified once the rats had not been breathing for 20 min. Interleukin-1β (IL-1β) (PI303, Beyotime), Interferon-β (IFNβ) (E-EL-R0545, Elabscience), Interferon-α (IFNα) (E-EL-R3036, Elabscience), malondialdehyde (MDA) (S0131S, Beyotime), superoxide dismutase (SOD) (E-EL-R1424, Elabscience), Immunoglobulin E (IgE) (E-EL-R0517, Elabscience), Immunoglobulin G1 (IgG1) (88-50500-88, Thermo Fisher Scientific), Immunoglobulin G2a (IgG2a) (E-EL-R2415, Elabscience) and glutathione (GSH) (E-EL-0026, Elabscience) levels were measured using the ELISA kits according to the manufacturer's instructions.

Western blot analysis of protein expression in the nasal mucosa. Nasal mucosa tissues were lysed with pre-cooled RIPA lysing solution (Beyotime Institute of Biotechnology; cat. no. P0013B; 89% RIPA+10% 10X cocktail+1% PMSF) and protein concentration was determined by BCA assay. Proteins (20 μg of protein was added to each lane) were separated by SDS-PAGE on 12% gels and were transferred to PVDF membranes. The membranes were blocked with 5% non-fat milk at room temperature for 2 h, and were then incubated overnight with primary antibodies (p-AMPK (Abcam; cat. no. ab133448; 1:1,000), t-AMPK (Abcam; cat. no. ab32047; 1:1,000), p-STING (Abcam; cat. no. ab318182; 1:1,000), t-STING (Abcam; cat. no. ab227128; 1:1,000), p-TBK1 (CST, cat. no. 5483; 1:1,000), t-TBK1 (CST, cat. no. 38066; 1:1,000), p-SHP1 (CST, cat. no. 47696; 1:1,000), t-SHP1 (CST, cat. no. 26516; 1:1,000), p-SHP2 (CST, cat. no. 5431; 1:1,000), t-SHP2 (CST, cat. no. 3397; 1:1,000), NOX4 (Beyotime, AF1498; 1:1,000), NLRP3 (Abcam; cat. no. ab263899; 1:1,000), IFNβ (Beyotime Institute of Biotechnology; cat. no. AF7170; 1:1,000), GAPDH (Abcam; cat. no. ab181602; 1:1,000)) and with secondary antibodies (Goat anti-rabbit IgG H&L (HRP), Abcam; cat. no. ab6721; 1:2,000) for 1 h at room temperature. ECL detection kit (Beyotime Institute of Biotechnology; cat. no. P0018M) was used to visualize the protein bands. Greyscale analysis was performed using GAPDH as a loading control. ImageJ was used to analyze the bands (National Institutes of Health, 1.8.0).

Cell model construction and grouping. A 15-ml conical tube containing 3 ml complete culture medium [10% fetal bovine serum (Beyotime Institute of Biotechnology; cat. no. C0226) and 1% penicillin/streptomycin solution (Beyotime Institute of Biotechnology; cat. no. C0222)] was prepared for the macrophages obtained from 5 normal rats (these 5 rats were separated from the 32 rats that were divided into four groups.).

Bronchoalveolar lavage (BAL) buffer (PBS + EDTA) was heated to 37˚C in a water bath, taking care to maintain the temperature throughout the process. Anesthesia was first induced in rats using 4.5% isoflurane and then maintained using 2% isoflurane. After the rats were fully anesthetized, they were transferred to a CO_2 euthanasia chamber and CO_2 was introduced at 30% chamber volume/min; the concentration was gradually increased until the rats stopped breathing. The rats continued to be exposed to CO_2 for 1 min to ensure that the rats were dead. Subsequently, the skin, chest cavity, and muscles of the rats were excised using a dissection tool, and the lungs and trachea were exposed to avoid cutting or rupturing blood vessels. A pair of fine scissors was used to make a small incision in the upper part of the trachea just below the larynx; the downward-facing part of the trachea was left intact without cutting the entire trachea. A slightly blunt 18-G cannula was inserted through the incision, and the cannula was inserted deeper into the trachea toward the lungs taking care not to damage the lung tissue. A 1-ml syringe of warm BAL buffer was attached to the inserted cannula, the buffer was injected and the cannula was secured in position. Subsequently, the plunger was pulled to collect the BAL solution from the syringe. The collected BAL solution was filtered through a 70-μm cell strainer into a 15-ml tube containing 3 ml complete medium. The supernatant was removed by centrifugation at 300 x g and 4˚C for 5 min. Residual erythrocytes were lysed by adding 1 ml lysogeny solution (Beyotime Institute of Biotechnology; cat. no. C3702) and incubating for 2 min at room temperature. An appropriate amount of complete medium was added to the tube, lysis was terminated, the cells were collected by centrifugation (300 x g for 5 min at room temperature) and the supernatant was removed (20). The collected alveolar macrophages were cultured *in vitro*. Alveolar macrophages were cultured in DMEM supplemented with 10% FBS and 1% penicillin/streptomycin (Gibco; Thermo Fisher Scientific, Inc.). The cells were incubated at 37˚C, 5% CO_2 and 95% humidity. Alveolar macrophages were identified using immunofluorescence.

Macrophages were divided into the following six groups: i) Negative control (NC) group: Macrophages without treatment; ii) LPS and IFN-γ group: Macrophages treated with 1 μg/ml LPS and 20 ng/ml IFN-γ; iii) LPS + IFN-γ + HPE group: Macrophages treated with LPS (1 μg/ml), IFN-γ (20 ng/ml) and HPE (40 ng/ml); iv) LPS + IFN-γ + HPE + AMPK inhibitor group: Macrophages treated with LPS, IFN-γ, HPE and the AMPK inhibitor dorsomorphin 2HCl (5 μM); v) LPS + IFN-γ + HPE + NSC-87877 group: Macrophages treated with LPS, IFN-γ, HPE and the dual inhibitor NSC-87877 (5 μM); vi) LPS + IFN-γ + HPE + DMXAA group: Macrophages treated with LPS, IFN-γ, HPE and the STING agonist DMXAA (100 μg/ml). The above reagents were treated for 24 h at room temperature.

The protein expression levels in these cell groups were assessed by western blotting, as aforementioned, and the levels of IL-1β, IFNβ, IFNα, MDA, SOD and GSH in the culture supernatant of the cells groups were measured using ELISA kits as aforementioned.

Immunofluorescence staining. First, coverslips were washed and sterilized, and were then placed in a 24-well plate, inoculated with a macrophage suspension of appropriate density (~1x10^5 cells/ml), and incubated for 48 h at 37˚C with 5% CO_2 until the cells adhered to the wall. Next, the cells were washed with PBS, fixed with 4% paraformaldehyde for 15 min at room temperature and washed again with PBS. Finally, a drop of sealer was added to the slide, and the coverslip was covered with the cell side down and fixed with sealing adhesive. The operation was carried out with attention to aseptic conditions, cell density control and avoiding air bubbles when sealing the slides. The sections were then baked in an oven at 65˚C for 1 h. The sections were deparaffinized by soaking them in xylene twice (10 min each time). The sections were then soaked twice in anhydrous ethanol (5 min each) and were incubated in different ethanol concentrations (95, 90, 85, 80 and 75% ethanol; 2 min each), before being rinsed under running water, and washed and soaked in 1X PBS. Subsequently, the sections were completely soaked in citric acid antigen repair solution containing EDTA, boiled at 200˚C for 150 sec, cooled at room temperature, and then removed and soaked in distilled water for 3 min. The sections were then soaked in 3% hydrogen peroxide solution for 10 min to fully block endogenous peroxidase and washed in distilled water (room temperature). The sections were incubated with diluted anti-CD68 primary antibody (Abcam; cat. no. ab955; 1:50) overnight at 4˚C in a wet box. The following day, the incubated sections were washed three times with PBS (5 min each), were shaken dry, and a FITC-conjugated secondary antibody (Abcam; cat. no. ab150113; 1:200) was added dropwise, before being incubated for 50 min at room temperature. The sections were then washed three times with PBS (5 min each), were air-dried at room temperature, and the DAPI staining solution was added dropwise, before being incubated for 10 min at room temperature. Subsequently, the sections were dried, and then sealed with an anti-fluorescent quenching sealer. The sections were observed under a fluorescence microscope and the images were collected.

Transwell assay. Macrophages were seeded into the upper chamber of a Transwell system (6-well plate, 24 mm) at a density of 1x10^5 cells/well, and DMEM containing 10% FBS was added to the lower chamber. After 24 h, the cells in the lower chamber were removed, fixed with 4% methanol (room temperature, 15 min) and stained with 0.5% crystal violet (room temperature, 10 min). Cell migration was recorded using a light microscope x10 objective, and migration numbers were assessed using ImageJ software (National Institutes of Health, 1.8.0).

Statistical analysis. GraphPad Prism 9 (Dotmatics) was used for the statistics and the experiments were repeated three times. Data were presented as the mean ± standard error of the mean. One-way ANOVA was used for comparisons between groups, followed by Tukey's HSD post hoc test. $P<0.05$ was considered to indicate a statistically significant difference.

Results

DEG expression analysis between allergic rhinitis and healthy controls in the GSE44037 dataset. During the data preprocessing stage, the consistency of the distribution of

normalized expression levels across samples was first verified using box plots (Fig. 1A). Next, principal component analysis (PCA) was used to visually assess batch effects and it showed a significant improvement in sample clustering after Combat correction (Fig. 1B). For the GSE44037 dataset, differential expression analysis was conducted between the allergic rhinitis group and the healthy controls using the limma package. Strict criteria of |log2FC|>1 and FDR <0.05 was applied, which led to the identification of 207 significantly DEGs from the volcano plot. Among these, 166 genes were upregulated and 41 genes were downregulated (Fig. 1C). The differential gene expression patterns were further visualized using a hierarchical clustering heatmap (Fig. 1D). The GO analysis indicated that the DEGs were enriched in the CC terms 'npBAF complex', 'nBAF complex' and 'ATPase complex'; in the MF terms 'nucleosomal DNA binding', 'chromatin DNA binding' and 'transcription corepressor activity'; and in the BP terms 'positive regulation of DNA-binding transcription factor activity', 'inflammatory cell apoptotic process' and 'positive regulation of NF-kappaB transcription factor activity' (Fig. 1E). KEGG pathway analysis further revealed significant enrichment of DEGs in the 'AMPK signaling pathway' (Fig. 1F). The dataset GSE44037 identified positive correlations among several differential genes: AMPK (PRKAA2) and NF-κB (RELA) (Fig. 1G), AMPK (PRKAA2) and PU.1 (SPI1) (Fig. 1H), PU.1 (SPI1) and SHP1 (NSFL1C) (Fig. 1I), and NF-κB (RELA) and SHP2 (PTPN11) (Fig. 1J). Furthermore, there was a negative correlation between SHP2 (PTPN11) and TBK1 (Fig. 1K), along with a positive correlation between TBK1 and IRF3 (Fig. 1L).

HPE alleviates AR-induced inflammatory damage and is associated with AMPK. Histological examination via H&E staining showed that the sham group exhibited intact tissue structure with no notable pathological changes (Fig. 2A). The model group exhibited pathological phenomena, including extensive inflammatory cell infiltration, tissue detachment and edema. In the model + HPE group, tissue structure gradually recovered, with a reduction in edema and inflammatory infiltration. Compared with in the model + HPE group, the model + HPE + AMPK inhibitor group exhibited marked pathological damage. Furthermore, serum levels of IgE, IgG1, IgG2a, IL-1β and IFNβ were significantly elevated in the model group compared with those in the sham group, whereas these levels were significantly decreased in the model + HPE group compared with those in the model group. However, in the model + HPE + AMPK inhibitor group, the serum levels of IgE, IgG1, IgG2a, IL-1β and IFNβ were significantly increased compared with those in the model + HPE group, with no significant differences observed between the model and model + HPE + AMPK inhibitor groups (Fig. 2B). The expression levels of CD68 were further detected by immunofluorescence, and it was revealed that the expression levels of CD68 were elevated in the model group compared with those in the sham group, and were decreased in the model + HPE group compared with in the model group, whereas the addition of an AMPK inhibitor increased the expression levels of CD68 (Fig. 2C).

HPE acts on AMPK, promoting SHP1/SHP2 protein expression and suppressing STING/TBK1 expression in nasal mucosal tissue. Compared with in the sham group, the model group exhibited decreased expression of phosphorylated (p)-AMPK/total (t)-AMPK, p-SHP1/t-SHP1 and p-SHP2/t-SHP2, whereas p-STING/t-STING and p-TBK1/t-TBK1 expression levels were elevated. In the model + HPE group, the levels of p-AMPK/t-AMPK, p-SHP1/t-SHP1 and p-SHP2/t-SHP2 were increased, whereas those of p-STING/t-STING and p-TBK1/t-TBK1 were decreased compared with those in the model group. In the model + HPE + AMPK inhibitor group, p-AMPK/t-AMPK, p-SHP1/t-SHP1 and p-SHP2/t-SHP2 levels were decreased, whereas p-STING/t-STING and p-TBK1/t-TBK1 were increased compared with those in the model + HPE group (Fig. 3).

HPE alleviates inflammatory responses, and reduces cell apoptosis and migration in rat macrophages. Research has shown that the mechanism by which macrophages act in AR significantly affects the inflammatory response of the nasal mucosa and the levels of immune factors through the inflammatory mediators they produce. This includes promoting nasal mucosal inflammation by secreting Th2-type cytokines (such as IL-4, IL-5 and IL-13) and regulating the levels of immune factors in serum, further supporting the key role of macrophages in AR (21,22). Macrophages are the primary regulators in initiating immune responses, whereas other cells participate in local and systemic inflammatory responses through synergistic or auxiliary mechanisms. The results of immunofluorescence staining of CD68 confirmed the success of alveolar macrophage extraction (Fig. 4A). In this study, alveolar macrophages from normal rats were isolated and subjected to *in vitro* experiments. Western blot analysis (Fig. 4B and C) revealed that the LPS + IFN-γ group showed significantly elevated levels of NOX4, p-STING/t-STING, p-TBK1/t-TBK1, NLRP3, and IFNβ, but reduced p-AMPK/t-AMPK, p-SHP1/t-SHP1, and p-SHP2/t-SHP2 compared with the NC group. The LPS + IFN-γ + HPE group exhibited decreased levels of NOX4, p-STING/t-STING, p-TBK1/t-TBK1, NLRP3, and IFNβ, alongside increased p-AMPK/t-AMPK, p-SHP1/t-SHP1, and p-SHP2/t-SHP2. Conversely, the LPS + IFN-γ + HPE + AMPK inhibitor group displayed elevated NOX4, p-STING/t-STING, p-TBK1/t-TBK1, NLRP3, and IFNβ, with reduced p-AMPK/t-AMPK, p-SHP1/t-SHP1, and p-SHP2/t-SHP2. The LPS + IFN-γ + HPE + DMXAA group had higher NOX4, p-STING/t-STING, p-TBK1/t-TBK1, NLRP3, and IFNβ levels compared with the LPS + IFN-γ group, but lower p-AMPK/t-AMPK, p-SHP1/t-SHP1, and p-SHP2/t-SHP2. Additionally, the LPS + IFN-γ + HPE + DMXAA group showed increased NOX4, p-STING/t-STING, p-TBK1/t-TBK1, NLRP3, and IFNβ, and decreased p-AMPK/t-AMPK, p-SHP1/t-SHP1, and p-SHP2/t-SHP2 compared with the LPS + IFN-γ + HPE group. Compared with the LPS + IFN-γ + HPE + AMPK inhibitor and LPS + IFN-γ + HPE + NSC-87877 groups, the LPS + IFN-γ + HPE + DMXAA group demonstrated elevated NOX4, p-STING/t-STING, p-TBK1/t-TBK1, NLRP3, and IFNβ, with reduced p-AMPK/t-AMPK, p-SHP1/t-SHP1, and p-SHP2/t-SHP2.

ELISA results (Fig. 4D and E) showed that the LPS + IFN-γ group had elevated levels of IL-1β, IFNβ, IFNα, and MDA, but reduced SOD and GSH compared with the NC group. The LPS + IFN-γ + HPE group exhibited decreased IL-1β, IFNβ, IFNα, and MDA, and increased SOD and GSH.

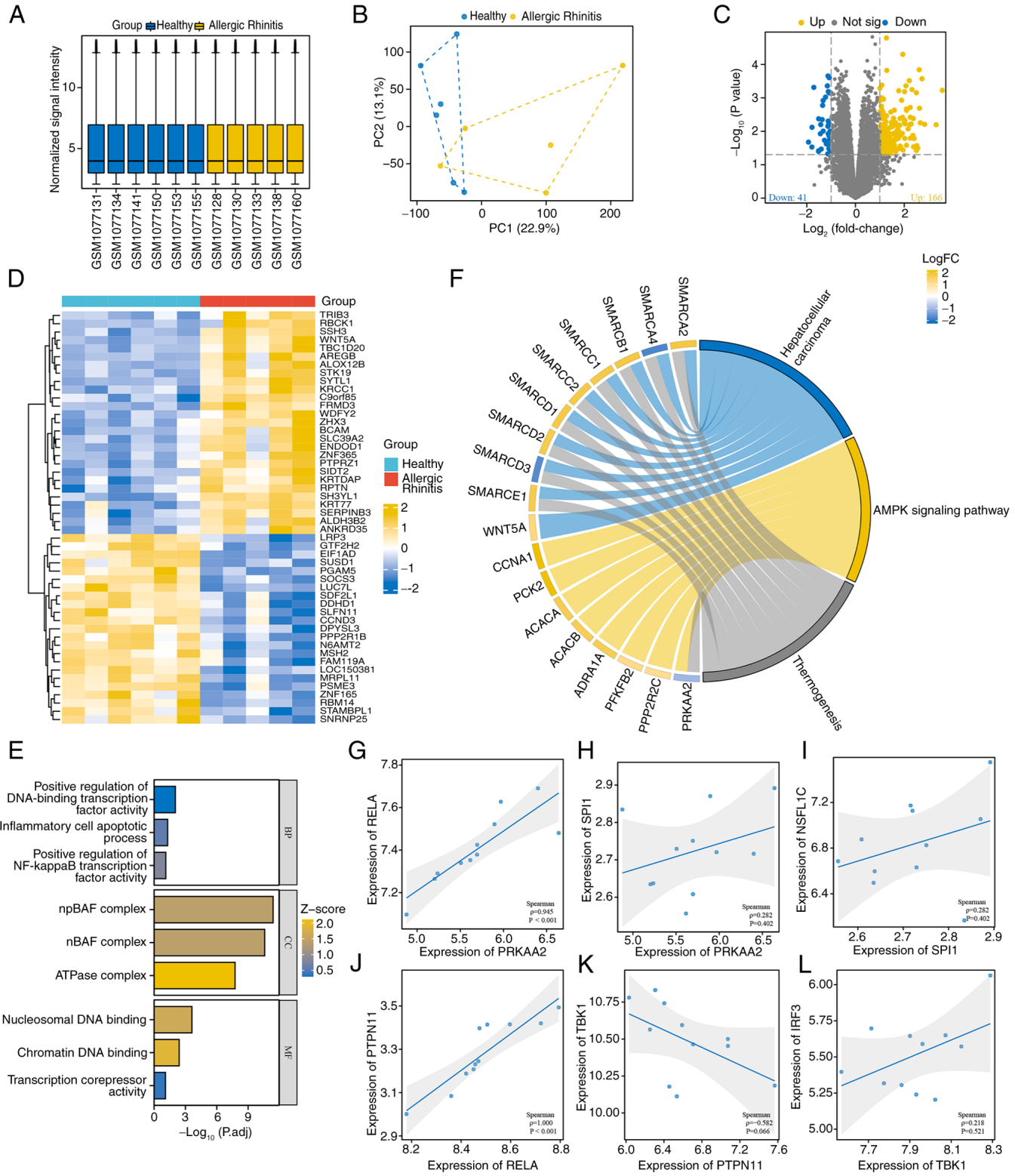

Figure 1. Bioinformatics analysis. (A) Sample normalization boxplot. (B) Principal component analysis plot showing the differences between samples. (C) Volcano plot of DEGs. (D) Heatmap of DEGs. (E) Bar chart of Gene Ontology enrichment analysis. (F) Chord diagram of Kyoto of Encyclopedia of Genes and Genomes enrichment analysis. Scatter plots of (G) AMPK and NF-κB correlation, (H) AMPK and PU.1 correlation, (I) PU.1 and SHP1 correlation, (J) NF-κB and SHP2 correlation, (K) SHP2 and TBK1 correlation and (L) TBK1 and IRF3 correlation. DEGs, differentially expressed genes; SHP, Src homology 2-containing phosphatase.

In contrast, the LPS + IFN-γ + HPE + AMPK inhibitor group displayed higher IL-1β, IFNβ, IFNα, and MDA, and lower SOD and GSH. The LPS + IFN-γ + HPE + DMXAA group showed elevated IL-1β, IFNβ, IFNα, and MDA, and reduced SOD and GSH compared with both the LPS + IFN-γ group and the LPS + IFN-γ + HPE group. . Compared with the LPS + IFN-γ + HPE + AMPK inhibitor group, IL-1β, IFNβ, IFNα and MDA levels were elevated and SOD and GSH levels

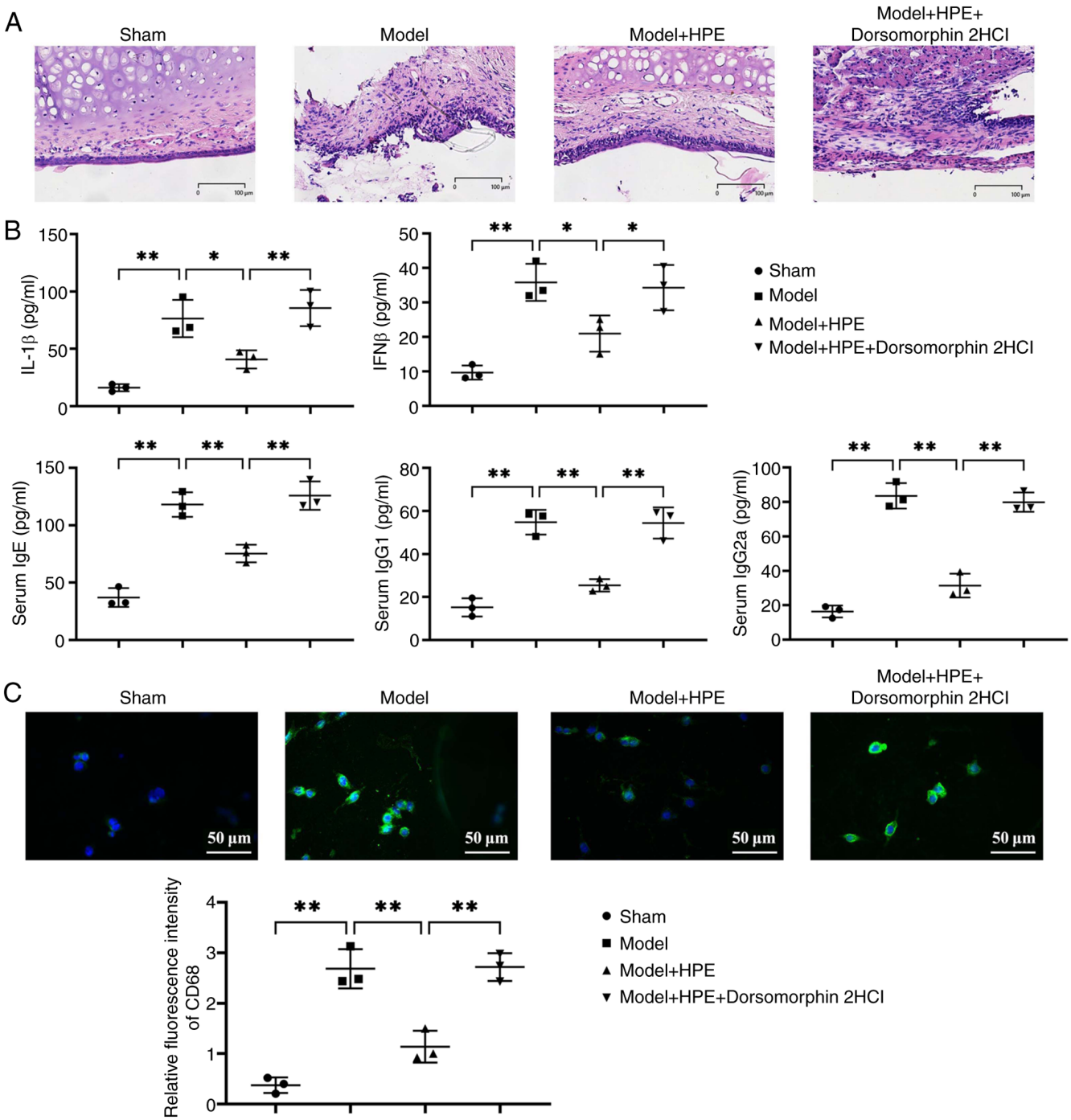

Figure 2. HPE can alleviate allergic rhinitis damage, with AMPK serving a notable role. (A) Hematoxylin and eosin staining of nasal mucosal tissues. (B) ELISA was used to detect IL-1β, IFNβ, IgE, IgG1 and IgG2 levels in the serum of rats. (C) Immunofluorescence was used to detect the expression levels of CD68 in the rats. **P<0.01, *P<0.05. HPE, human placental extracts; IFN, interferon; Ig, immunoglobulin. **P<0.01, *P<0.05.

were decreased in the LPS + IFN-γ + HPE + DMXAA group. These results suggested that HPE attenuated the inflammatory response in rat macrophages by mediating the reactive oxygen species (ROS)/AMPK/SHP1/SHP2/STING signaling pathway.

The important role of macrophage migration in nasal mucosal remodeling was assessed in the present study, as macrophages migrating to the site of inflammation can influence the expression of signaling pathway proteins (23). Additionally, the signaling factors released by apoptotic macrophages can be recognized by other immune cells, thus affecting the levels of immune factors in both the nasal mucosa and serum. Therefore, Transwell migration experiments were conducted on macrophages from different groups. In the Transwell experiment (Fig. 5A and B), compared with in the NC group, cell migration was increased in the LPS + IFN-γ group; however, when compared with the LPS + IFN-γ group, cell migration was decreased in the LPS + IFN-γ + HPE group. In addition, when compared with the LPS + IFN-γ + HPE group, cell migration was increased in the LPS + IFN-γ + HPE + AMPK inhibitor group, and when compared with the LPS + IFN-γ group, cell migration was increased in the LPS + IFN-γ + HPE + DMXAA group. Furthermore, when compared

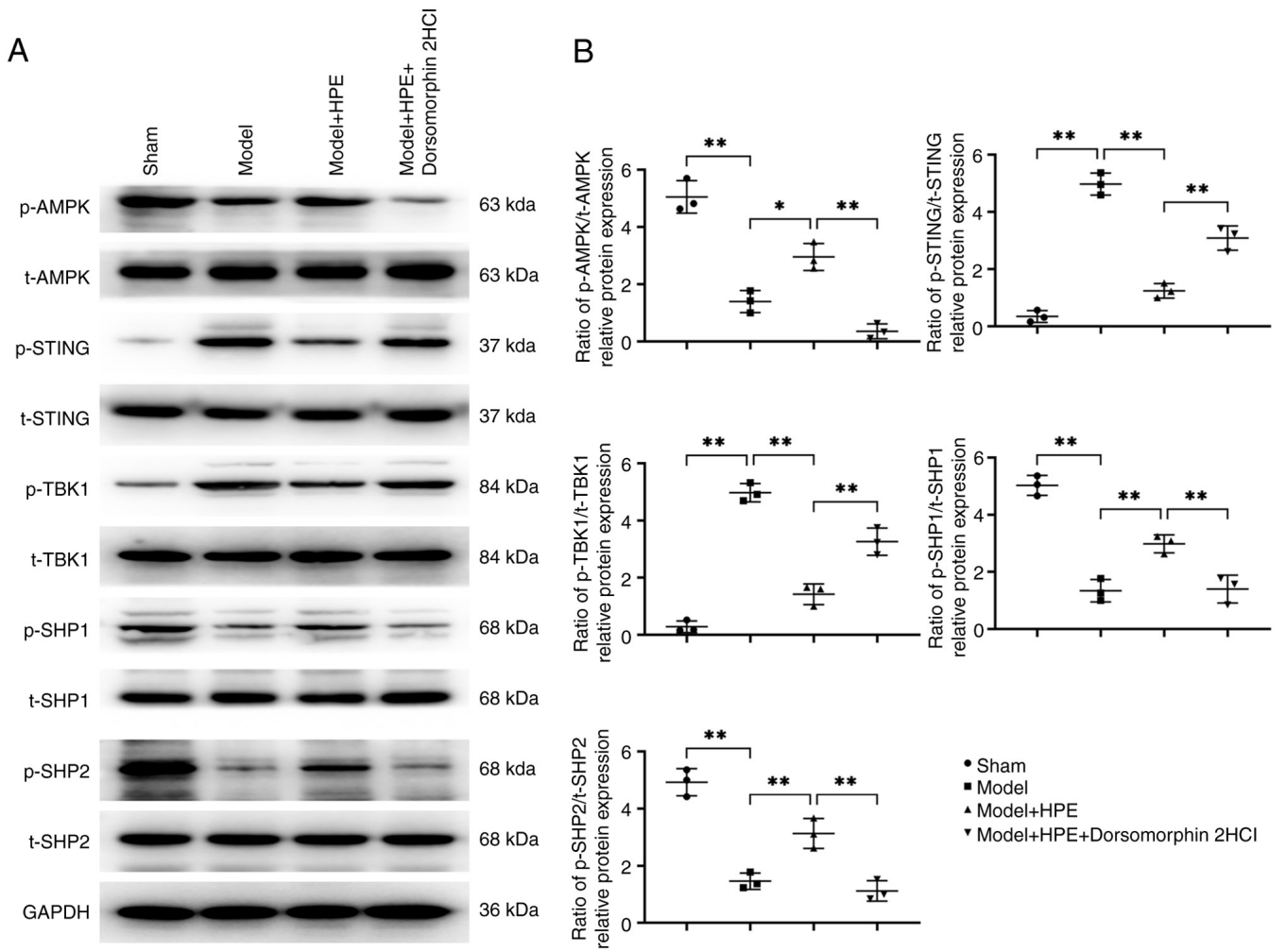

Figure 3. HPE acts on AMPK and promotes SHP1/SHP2 protein expression while inhibiting STING/TBK1 expression. (A) Protein banding maps of p-AMPK, t-AMPK, p-STING, t-STING, p-TBK1, t-TBK1, p-SHP1, t-SHP1, and p-SHP2, t-SHP2 were detected in nasal mucosal tissues by Western blot analysis. (B) Western blot analysis was performed to detect the protein expression levels of p-AMPK/t-AMPK, p-STING/t-STING, p-TBK1/t-TBK1, p-SHP1/t-SHP1 and p-SHP2/t-SHP2 in nasal mucosal tissues. $^{**}P<0.01$, $^{*}P<0.05$. HPE, human placental extracts; p-, phosphorylated; SHP, Src homology 2-containing phosphatase; t-t, total.

with the LPS + IFN-γ + HPE, LPS + IFN-γ + HPE + AMPK inhibitor and LPS + IFN-γ + HPE + NSC-87877 groups, cell migration was significantly increased in the LPS + IFN-γ + HPE + DMXAA group. HPE promotes the NF-κB signaling pathway through activation of AMPK, and NF-κB directly activates SHP2 on the one hand, and SHP1 on the other hand via C/EBPα/PU.1. SHP1 inhibits STING, and SHP2 inhibits TBK1, thereby inhibiting the STING/TBK1 signaling pathway, which mediates inflammatory responses and promotes mitochondrial via IRF3 Oxidative Stress. Mitochondrial oxidative stress upregulates the expression of cGAMP and P53: cGAMP binds to STING and stabilizes its dimers and oligomers; P53 inhibits SHP1 and SHP2, and promotes the expression of both SYK and EGFR. STING interacts with EGFR, leading to the autophosphorylation of EGFR and activation of SYK, which then phosphorylates STING and EGFR at Y240 and Y245 sites, respectively. SYK and EGFR phosphorylate STING at the Y240 and Y245 sites, respectively, promoting its translocation to ERGIC for signaling. In conclusion, HPE may inhibit AR by regulating the AMPK/SHP1/SHP2/STING signaling pathway (Fig. 6).

Discussion

AR is a chronic inflammatory disease of the nasal mucosa in sensitized individuals caused by a type I hypersensitivity reaction upon exposure to common allergens (24). The cascade of allergic inflammation serves a crucial role in the pathogenesis of AR. Inhaled allergens enter the nasal mucosa epithelial cells, triggering the release of a series of chemokines and the recruitment of immature dendritic cells, upregulating histone deacetylase activity, damaging tight junction proteins and compromising the integrity of the nasal mucosal epithelial barrier, thereby increasing the likelihood of allergen invasion (the process by which an allergen breaks through the epithelial barrier of the nasal mucosa, enters the body, and triggers an immune response) and exacerbating the allergic inflammatory response (25).

The results of the present study can be summarized as follows: i) OVA promotes the production of mitochondrial ROS (the present study examined the expression of MDA and NOX4), which in turn promotes the action of P53 (26). Mitochondrial damage leads to the production of cyclic

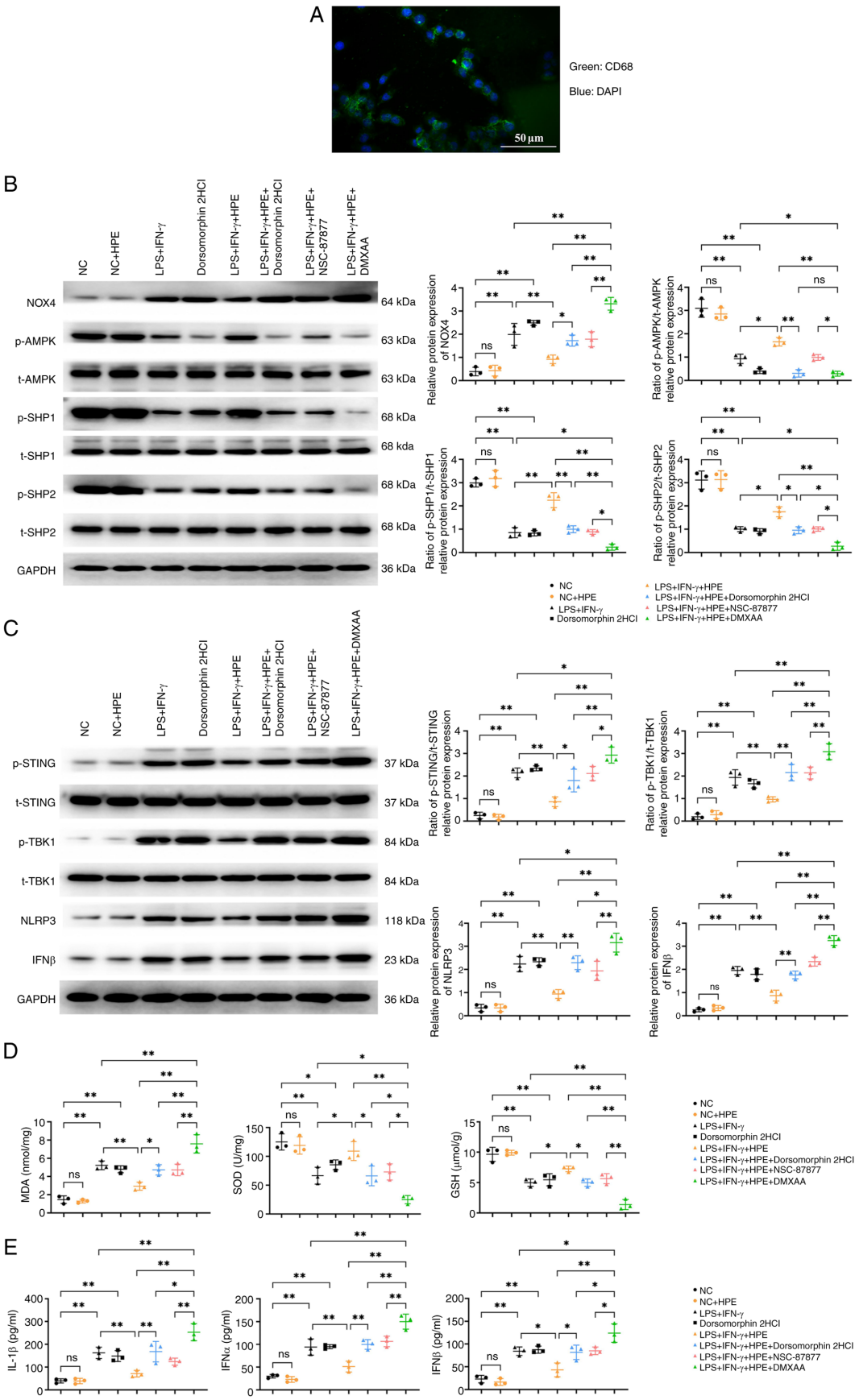

Figure 4. HPE alleviates the inflammatory response. (A) Immunofluorescence staining was used to detect extracted alveolar macrophages. (B) Western blot analysis was conducted to detect the protein expression levels of NOX4, p-AMPK/t-AMPK, p-SHP1/t-SHP1 and p-SHP2/t-SHP2 in macrophages. (C) Western blot analysis was conducted to detect the protein expression levels of p-STING/t-STING, p-TBK1/t-TBK1, NLRP3 and IFNβ in macrophages. ELISA was used to measure the levels of (D) MDA, SOD and GSH, and (E) IL-1β, IFNβ and IFNα in macrophage supernatants. **P<0.01, *P<0.05, ^{ns}P>0.05. GSH, glutathione; HPE, human placental extracts; IFN, interferon; LPS, lipopolysaccharide; MDA, malondialdehyde; NC, negative control; NOX4, NADPH oxidase 4; p-, phosphorylated; SHP, Src homology 2-containing phosphatase; SOD, superoxide dismutase; t-t, total.

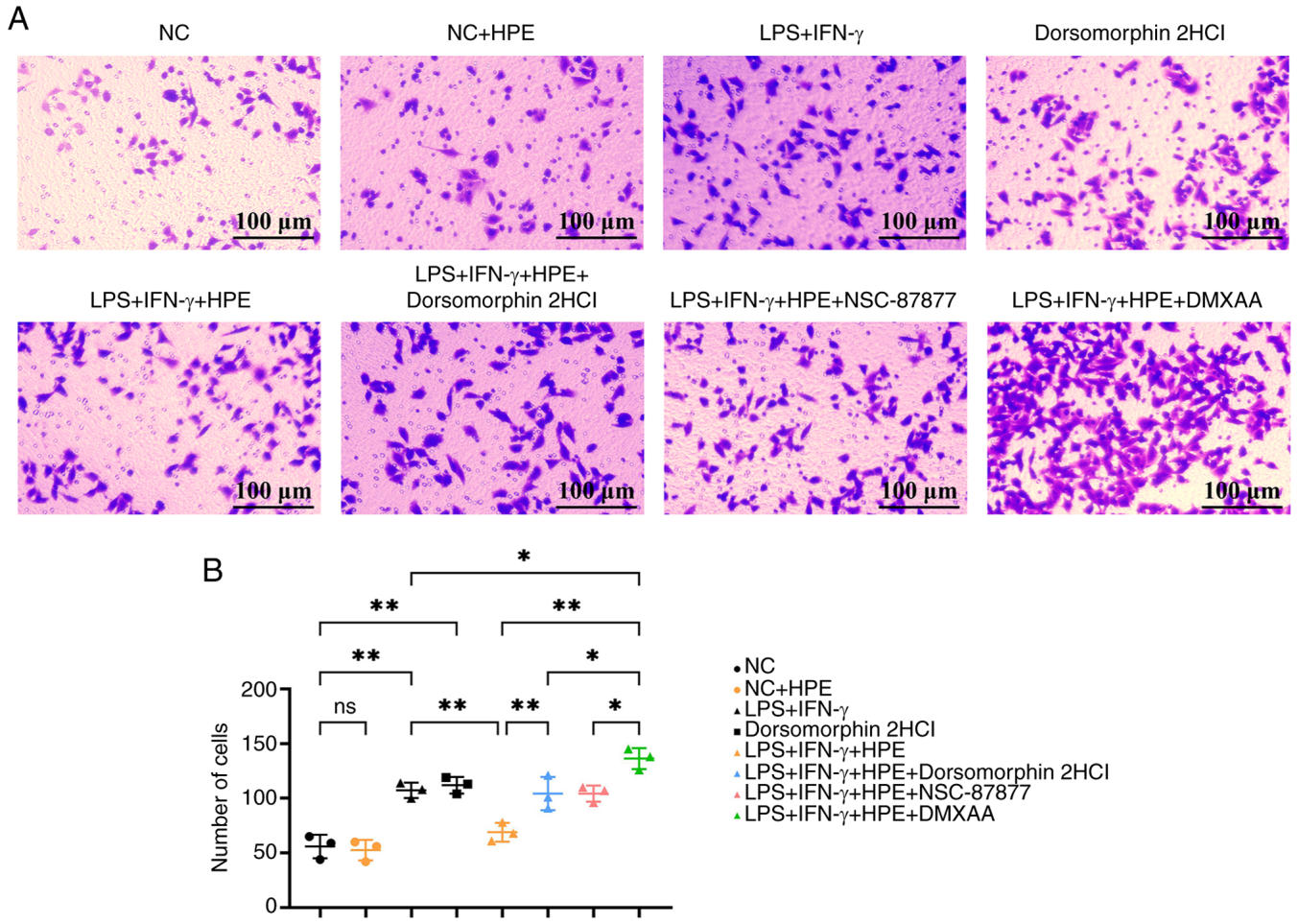

Figure 5. HPE reduces cell migration. (A) Transwell experiment assessed the migration of macrophages. (B) Statistical analysis of the migration assay. **P<0.01, *P<0.05. ns; not significant (P>0.05); HPE, human placental extracts; IFN, interferon; LPS, lipopolysaccharide; NC, negative control.

GMP-AMP (cGAMP) (27), which binds to STING and mediates the inflammatory response. ii) HPE inhibits ROS activity (the present study examined the expression of MDA and NOX4) and promotes AMPK phosphorylation, which further acts on NF-κB to promote SHP1/SHP2 expression, thereby inhibiting the inflammatory response (9).

After OVA induces AR, it causes cells to produce large amounts of ROS, leading to oxidative stress (28). The main source of ROS is the mitochondrial respiratory chain, and when mitochondria are stimulated by external factors, the cellular ROS level increases. Excessive ROS, in turn, causes mitochondrial damage, which leads to more severe oxidative stress (29). When mitochondrial damage occurs, mitochondrial DNA (mtDNA) may be released from the mitochondria into the cytoplasm. In the cytoplasm, cGAS can recognize and bind to the free mtDNA; when cGAS binds to mtDNA, it undergoes a conformational change, which activates cGAS. Activated cGAS can then catalyze the synthesis of cGAMP from ATP and GTP (30). Meanwhile, high levels of ROS can cause DNA damage, which activates P53, and P53 can influence ROS levels by regulating a series of reactions. Upon activation, P53 directs the cell to repair DNA damage or induce apoptosis to prevent damaged cells from continuing to proliferate; however, in certain situations, such as under stress conditions, activation of P53 can lead to further increases in ROS levels, forming a positive feedback loop that enhances P53 activation and the apoptotic process. Spleen tyrosine kinase (SYK) is a non-receptor tyrosine kinase involved in signal transduction and regulation of cellular functions. It has previously been shown that P53 can directly or indirectly influence SYK expression through transcriptional regulatory mechanisms (31). Epidermal growth factor receptor (EGFR) is an important receptor tyrosine kinase involved in the regulation of cell proliferation, differentiation and survival. In certain cases, P53 and the EGFR signaling pathway may coordinate to regulate cellular stress responses and inflammatory responses (32). In the present study, P53 promoted SYK transcription, which acted on the STING phosphorylation site, and P53 also acted on the EGFR promoter, thereby affecting the STING phosphorylation site, as shown in Figs. 3 and 4). As a second messenger, cGAMP binds to and activates STING on the endoplasmic reticulum membrane. Activated STING translocates to the Golgi apparatus, and recruits and activates multiple downstream effectors, including TBK1 and IKKε (33). These effectors further phosphorylate and activate IFN regulatory factor 3 (IRF3), and phosphorylated IRF3 acts on the promoters of inflammatory factors, such as NLRP3 and IFNα/β, leading to their upregulation, further promoting ROS expression and forming a vicious cycle (34-36).

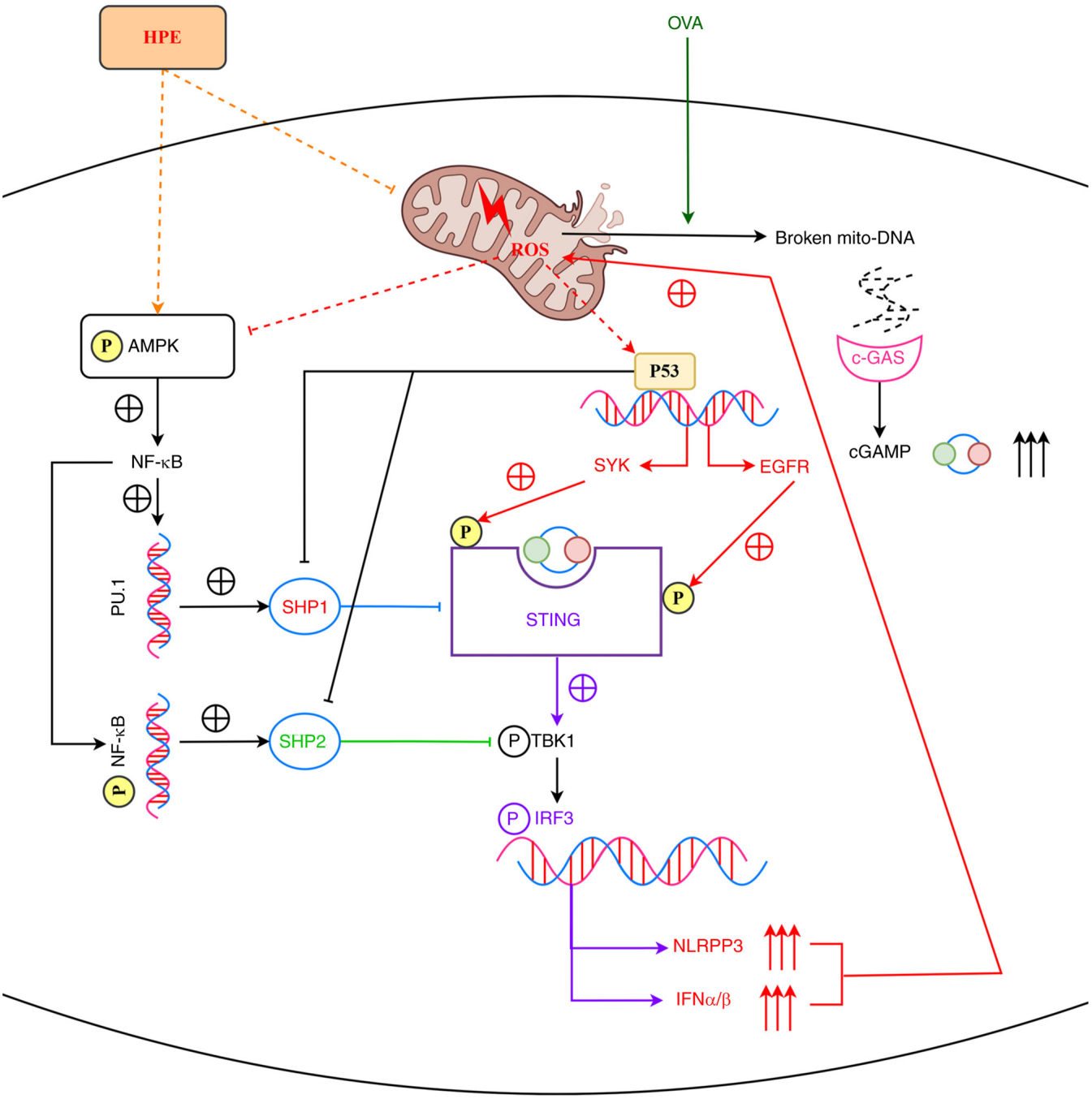

Figure 6. HPE inhibits allergic rhinitis by modulating the AMPK/SHP1/SHP2/STING signaling pathway. HPE promotes the NF-κB signaling pathway through activation of AMPK, and NF-κB directly activates SHP2 on the one hand, and SHP1 on the other hand via C/EBPα/PU.1. SHP1 inhibits STING, and SHP2 inhibits TBK1, thereby inhibiting the STING/TBK1 signaling pathway, which mediates inflammatory responses and promotes mitochondrial via IRF3 Oxidative Stress. Mitochondrial oxidative stress upregulates the expression of cGAMP and P53: cGAMP binds to STING and stabilizes its dimers and oligomers; P53 inhibits SHP1 and SHP2, and promotes the expression of both SYK and EGFR. STING interacts with EGFR, leading to the autophosphorylation of EGFR and activation of SYK, which then phosphorylates STING and EGFR at Y240 and Y245 sites, respectively. SYK and EGFR phosphorylate STING at the Y240 and Y245 sites, respectively, promoting its translocation to ERGIC for signaling. cGAMP, cyclic GMP-AMP; EGFR, epidermal growth factor; HPE, human placental extracts; IFN, interferon; IRF3, IFN regulatory factor 3; OVA, ovalbumin; SHP, Src homology 2-containing phosphatase; SYK, spleen tyrosine kinase.

HPE is rich in active substances such as peptides, cytokines and amino acids. Peptides promote cell signaling, enhance cell proliferation and differentiation, and thus contribute to tissue repair and regeneration. Amino acids are the basic building blocks of proteins, and serve key roles in wound healing, anti-inflammation and antioxidant processes. Growth factors, including EGF and insulin-like growth factor, accelerate wound healing and tissue regeneration by activating receptors on the cell surface and promoting matrix protein synthesis (37). Therefore, the antioxidant effect of HPE may be due to the action of amino acids (38). HPE acts on cells through endocytosis to treat AR. The western blot and ELISA assays also showed that HPE inhibited ROS activity, and bioinformatics analysis revealed that HPE

promotes AMPK phosphorylation, and p-AMPK promotes NF-κB activity (Figs. 3 and 4). In a non-inflammatory state, activated AMPK promotes the expression of antioxidant factors through NF-κB and inhibits STING expression via SHP1, thereby reducing the inflammatory response (39). In an inflammatory state, STING activates NF-κB, exacerbating the inflammatory response. AMPK inhibits TBK1 activity by promoting SHP2 expression, indirectly inhibiting the STING signaling pathway. ROS inhibits AMPK phosphorylation, reducing the AMPK-induced promotion of NF-κB, thereby indirectly affecting the inflammatory response; P53 inhibits SHP1 and SHP2, relieving inhibition of STING and TBK1, thereby enhancing the inflammatory response, so the two pathways, SHP2/SHP1 and STING/TBK1, mutually inhibit each other (39,40).

In conclusion, HPE may inhibit AR by modulating AMPK/SHP1/SHP2/STING signaling. This provides a therapeutic target for the treatment of AR; however, relevant clinical studies are needed to provide a more robust basis for this conclusion. This study illustrates that HPEs have potential clinical significance, such as providing new therapeutic strategies for prostate cancer or allergic diseases, and may be suitable for long-term use and personalized therapy due to their multi-target modulation and natural compound advantages. However, relevant clinical trials are needed to provide a stronger basis for the conclusions of this study.

Acknowledgements

Not applicable.

Funding

No funding was received.

Availability of data and materials

The data generated in the present study may be requested from the corresponding author.

Authors' contributions

BW contributed to the conception and design of the study, organized the AR dataset GSE44037 and wrote the first draft of the manuscript. SL conducted statistical analysis of the data. ZL and XL carried out experiments. All authors participated in the revision of the manuscript and read and approved the final version of the manuscript. BW and SL confirm the authenticity of all the raw data.

Ethics approval and consent to participate

The present study was approved by the Animal Protection and Use Committee of Hebei Medical University (approval no. IACUC-Hebmu-P-2024024).

Patient consent for publication

Not applicable.

Competing interests

The authors declare that they have no competing interests.

References

1. Siddiqui ZA, Walker A, Pirwani MM, Tahiri M and Syed I: Allergic rhinitis: Diagnosis and management. Br J Hosp Med (Lond) 83: 1-9, 2022.
2. Schuler Iv CF and Montejo JM: Allergic rhinitis in children and adolescents. Pediatr Clin North Am 66: 981-993, 2019.
3. Pyun BJ, Lee JY, Kim YJ, Ji KY, Jung DH, Park KS, Jo K, Choi S, Jung MA, Kim YH and Kim T: Gardenia jasminoides Attenuates Allergic Rhinitis-induced inflammation by inhibiting periostin production. Pharmaceuticals (Basel) 14: 986, 2021.
4. Bjermer L, Westman M, Holmström M and Wickman MC: The complex pathophysiology of allergic rhinitis: Scientific rationale for the development of an alternative treatment option. Allergy Asthma Clin Immunol 15: 24, 2019.
5. De D, Chakraborty PD and Bhattacharyya D: Regulation of trypsin activity by peptide fraction of an aqueous extract of human placenta used as wound healer. J Cell Physiol 226: 2033-2040, 2011.
6. Lee JO, Jang Y, Park AY, Lee JM, Jeong K, Jeon SH, Jin H, Im M, Kim JW and Kim BJ: Human Placenta Extract (HPH) suppresses inflammatory responses in TNF-α/IFN-γ-Stimulated HaCaT cells and a DNCB atopic dermatitis (AD)-like mouse model. J Microbiol Biotechnol 34: 1969-1980, 2024.
7. Hackethal J, Weihs AM, Karner L, Metzger M, Dungel P, Hennerbichler S, Redl H and Teuschl-Woller AH: Novel human Placenta-based extract for vascularization strategies in tissue engineering. Tissue Eng Part C Methods 27: 616-632, 2021.
8. Gwam C, Ohanele C, Hamby J, Chughtai N, Mufti Z and Ma X: Human placental extract: A potential therapeutic in treating osteoarthritis. Ann Transl Med 11: 322, 2023.
9. Samiei F, Jamshidzadeh A, Noorafshan A and Ghaderi A: Human placental extract ameliorates structural lung changes iinduced by amiodarone in rats. Iran J Pharm Res 15 (Suppl 1): S75-S82, 2016.
10. Lee YK, Chung HH and Kang SB: Efficacy and safety of human placenta extract in alleviating climacteric symptoms: Prospective, randomized, double-blind, placebo-controlled trial. J Obstet Gynaecol Res 35: 1096-1101, 2009.
11. Zhang W, Lu J, Wang Y, Sun P, Gao T, Xu N, Zhang Y and Xie W: Canagliflozin attenuates lipotoxicity in cardiomyocytes by inhibiting inflammation and ferroptosis through activating AMPK pathway. Int J Mol Sci 24: 858, 2023.
12. Zhang J, Sun Y, Tang K, Xu H, Xiao J and Li Y: RGC32 promotes the progression of ccRCC by activating the NF-κB/SHP2/EGFR signaling pathway. Aging (Albany NY): May 27, 2024 (Epub ahead of print).
13. Wang D, Paz-Priel I and Friedman AD: NF-kappa B p50 regulates C/EBP alpha expression and inflammatory cytokine-induced neutrophil production. J Immunol 182: 5757-5762, 2009.
14. Bi L, Yu Z, Wu J, Yu K, Hong G, Lu Z and Gao S: Honokiol inhibits constitutive and inducible STAT3 signaling via PU.1-Induced SHP1 expression in acute myeloid leukemia cells. Tohoku J Exp Med 237: 163-172, 2015.
15. Li BL, Zhao DY, Du PL, Wang XT, Yang Q and Cai YR: Luteolin alleviates ulcerative colitis through SHP-1/STAT3 pathway. Inflamm Res 70: 705-717, 2021.
16. Sun Z, Liu Q, Lv Z, Li J, Xu X, Sun H, Wang M, Sun K, Shi T, Liu Z, *et al*: Targeting macrophagic SHP2 for ameliorating osteoarthritis via TLR signaling. Acta Pharm Sin B 12: 3073-3084, 2022.
17. Zhang B, Zeng M, Zhang Q, Wang R, Jia J, Cao B, Liu M, Guo P, Zhang Y, Zheng X and Feng W: Ephedrae Herba polysaccharides inhibit the inflammation of ovalbumin induced asthma by regulating Th1/Th2 and Th17/Treg cell immune imbalance. Mol Immunol 152: 14-26, 2022.
18. Nur Husna SM, Md Shukri N, Tuan Sharif SE, Tan HTT, Mohd Ashari NS and Wong KK: IL-4/IL-13 axis in allergic rhinitis: Elevated serum cytokines levels and inverse association with tight junction molecules expression. Front Mol Biosci 9: 819772, 2022.
19. Shao YY, Zhou YM, Hu M, Li JZ, Chen CJ, Wang YJ, Shi XY, Wang WJ and Zhang TT: The Anti-allergic rhinitis effect of traditional Chinese medicine of Shenqi by regulating mast cell degranulation and Th1/Th2 cytokine balance. Molecules 22: 504, 2017.

20. Murray PJ and Wynn TA: Protective and pathogenic functions of macrophage subsets. Nat Rev Immunol 11: 723-737, 2011.
21. Hirano M, Ogita-Nakanishi H, Miyachi W, Hannya N, Yamamoto-Kimoto Y, Sakurai K, Miyoshi-Higashino M, Tashiro-Yamaji J, Kato R, Ijiri Y, *et al*: Essential role of macrophages in the initiation of allergic rhinitis in mice sensitized intranasally once with cedar pollen: Regulation of class switching of immunoglobulin in B cells by controlling interleukin-4 production in T cells of submandibular lymph nodes. Microbiol Immunol 56: 392-405, 2012.
22. Saradna A, Do DC, Kumar S, Fu QL and Gao P: Macrophage polarization and allergic asthma. Transl Res 191: 1-14, 2018.
23. Qu J, Sun Y, Liang N, Li C, Huang Q, Wang M, Wang D and Zhou B: Histopathological characteristics and inflammatory cell infiltration in sinonasal inverted papilloma. Am J Rhinol Allergy 39: 21-31, 2025.
24. Huang H, Ren Y, Liang H, Liu X, Nan J, Zhao H and Liu X: Mechanism of TCONS_00147848 regulating apoptosis of nasal mucosa cells and alleviating allergic rhinitis through FOSL2-mediated JAK/STAT3 signaling pathway. Sci Rep 11: 15991, 2021.
25. Geng B, Dilley M and Anterasian C: Biologic therapies for allergic rhinitis and nasal polyposis. Curr Allergy Asthma Rep 21: 36, 2021.
26. Zhou Y, Que KT, Zhang Z, Yi ZJ, Zhao PX, You Y, Gong JP and Liu ZJ: Iron overloaded polarizes macrophage to proinflammation phenotype through ROS/acetyl-p53 pathway. Cancer Med 7: 4012-4022, 2018.
27. Wang C, Sharma N, Veleeparambil M, Kessler PM, Willard B and Sen GC: STING-Mediated interferon induction by herpes simplex Virus 1 requires the protein tyrosine kinase syk. mBio 12: e0322821, 2021.
28. Meng L, Hao D, Liu Y, Yu P, Luo J, Li C, Jiang T, Yu J, Zhang Q, Liu S and Shi L: LRRC8A drives NADPH oxidase-mediated mitochondrial dysfunction and inflammation in allergic rhinitis. J Transl Med 22: 1034, 2024.
29. Drazdauskaitė G, Layhadi JA and Shamji MH: Mechanisms of allergen immunotherapy in allergic rhinitis. Curr Allergy Asthma Rep 21: 2, 2020.
30. Wen X, Tang L, Zhong R, Liu L, Chen L and Zhang H: Role of mitophagy in regulating intestinal oxidative damage. Antioxidants (Basel) 12: 480, 2023.
31. Jiménez-Loygorri JI, Villarejo-Zori B, Viedma-Poyatos Á, Zapata-Muñoz J, Benítez-Fernández R, Frutos-Lisón MD, Tomás-Barberán FA, Espín JC, Area-Gómez E, Gomez-Duran A and Boya P: Mitophagy curtails cytosolic mtDNA-dependent activation of cGAS/STING inflammation during aging. Nat Commun 15: 830, 2024.
32. Ho TLF, Lee MY, Goh HC, Ng GYN, Lee JJH, Kannan S, Lim YT, Zhao T, Lim EKH, Phua CZJ, *et al*: Domain-specific p53 mutants activate EGFR by distinct mechanisms exposing tissue-independent therapeutic vulnerabilities. Nat Commun 14: 1726, 2023.
33. Zajkowicz A, Gdowicz-Kłosok A, Krześniak M, Janus P, Łasut B and Rusin M: The Alzheimer's disease-associated TREM2 gene is regulated by p53 tumor suppressor protein. Neuroscie Lett 681: 62-67, 2018.
34. Yum S, Li M, Fang Y and Chen ZJ: TBK1 recruitment to STING activates both IRF3 and NF-κB that mediate immune defense against tumors and viral infections. Proc Natl Acad Sci USA 118: e2100225118, 2021.
35. Tanaka Y and Chen ZJ: STING specifies IRF3 phosphorylation by TBK1 in the cytosolic DNA signaling pathway. Sci Signal 5: ra20, 2012.
36. Duan N, Zhang Y, Tan S, Sun J, Ye M, Gao H, Pu K, Wu M, Wang Q and Zhai Q: Therapeutic targeting of STING-TBK1-IRF3 signalling ameliorates chronic stress induced depression-like behaviours by modulating neuroinflammation and microglia phagocytosis. Neurobiol Dis 169: 105739, 2022.
37. Wu T, He J, Yan S, Li J, Chen K, Zhang D, Cheng M, Xiang Z and Fang Y: Human placental extract suppresses mast cell activation and induces mast cell apoptosis. Allergy Asthma Clin Immunol 19: 98, 2023.
38. Jang SY, Park JW, Bu Y, Kang JO and Kim J: Protective effects of hominis placenta hydrolysates on radiation enteropathy in mice. Nat Prod Res 25: 1988-1992, 2011.
39. Liu C, Wang X, Qin W, Tu J, Li C, Zhao W, Ma L, Liu B, Qiu H and Yuan X: Combining radiation and the ATR inhibitor berzosertib activates STING signaling and enhances immunotherapy via inhibiting SHP1 function in colorectal cancer. Cancer Commun (Lond) 43: 435-454, 2023.
40. Ding H and Wu R: The Role of SHP2 in advancing COPD: Insights into oxidative stress, endoplasmic reticulum stress, and pyroptosis. Altern Ther Health Med: Apr 18, 2024 (Epub ahead of print).